Journal of Power Sources 199 (2012) 315–321

Contents lists available at SciVerse ScienceDirect

Journal of Power Sources

journal homepage: www.elsevier.com/locate/jpowsour

$NH_4V_3O_8$ nanorod as a high performance cathode material for rechargeable Li-ion batteries

Haiyan Wang[a,*], Yu Ren[b], Wenjie Wang[a], Xiaobing Huang[c], Kelong Huang[a,*], Yuan Wang[b], Suqin Liu[a]

[a] School of Chemistry and Chemical Engineering, Central South University, Changsha 410083, PR China
[b] School of Chemistry, University of St Andrews, Fife KY16 9ST, UK
[c] College of Chemistry and Chemical Engineering, Hunan University of Arts and Science, ChangDe 415000, PR China

ARTICLE INFO

Article history:
Received 1 August 2011
Accepted 17 October 2011
Available online 20 October 2011

Keywords:
Li-ion batteries
Ammonium trivanadate nanorod
Flake
Hydrothermal method
Sodium dodecyl benzene sulfonate
Electrochemical performance

ABSTRACT

A novel cathode material, $NH_4V_3O_8$ nanorods with high discharge capacity and good rate capability are hydrothermally prepared in the presence of sodium dodecyl benzene sulfonate (SDBS). The diameter of nanorods is about 30 nm and the length is less than 1 μm. In comparison with the ammonium trivanadate flakes prepared without surfactant, the nanorods are better suited as lithium inserting electrode material, with superior lithium ion insertion/deinsertion plateaus, higher discharge capacity and better cycling stability. The nanorods deliver a maximum specific discharge capacity of 327.1 mAh g^{-1} at 30 mA g^{-1}. It also demonstrates good rate capability with the capacity of 207.6 mAh g^{-1} at 300 mA g^{-1}, 201.2 mAh g^{-1} at 450 mA g^{-1}, and 181.8 mAh g^{-1} at 600 mA g^{-1}. Good cycling stability is also shown at 150 mA g^{-1} for the nanorods, with no capacity loss over 60 cycles.

1. Introduction

Li-ion batteries have been widely used in portable electronic devices and hold a great potential for utilization in powering electric vehicles (EVs) and hybrid electric vehicles (HEVs) due to their high energy density, high voltage, and long cycling life [1–5]. However, the energy and power density should be further improved to meet the current challenge of energy storage [1,6,7]. To achieve this goal, new materials with higher capacity and new nanomaterials chemistry are essential [8]. Over the past decade, nanostructuring has been considered one of the most powerful methods to improve electrochemical performance of electrode materials in terms of both energy and power densities, probably owning to their high surface-to-volume ratio, and short Li^+ diffusion distance [8–10].

Tremendous attention has been focused on vanadium oxides and their derivatives as cathode materials for Li-ion battery due to the easy synthesis, low cost and high capacity [11–16]. Of these materials, the most studied one is lithium trivanadate (LiV_3O_8), which possesses good structural stability. However, its electrochemical performance is strongly affected by the synthesis conditions and the possible following thermal treatment [17,18]. Meantime, it is noted that Li^+ in LiV_3O_8 usually occupy the octahedral sites in the interlayer, which are immobile. For this reason, other cations with larger ionic radius, such as NH_4^+, Na^+ and K^+ could substitute the Li^+ in $V_3O_8^-$ layers to form new electrode materials, which are expected to possess the larger path for Li+ intercalation and deintercalation [19–21]. Recently, we have fabricated the $NH_4V_3O_8$ flakes with the thickness of 500–600 nm [21]. It shows a discharge capacity of about 300 mAh g^{-1}. However, it is found that the large thickness of the flakes hinders the movement of lithium ion, which limits the rate capability. Furthermore, the abnormal lithium insertion potential (less than 2.0 V) into the host reveals the lower energy density as cathode material. Therefore, $NH_4V_3O_8$/CNTs composite is fabricated, which shows a high discharge capacity up to 358.7 mAh g^{-1} at 30 mA g^{-1} and excellent cycling stability [21]. Several other groups [22–24] have reported the preparation of $NH_4V_3O_8$ so far. However, only one paper mentioned the electrochemical performance of this kind material as lithium intercalated electrode [24]. Torardi and Miao [24] once introduced the F substituted ammonium trivanadate, $(NH_4)_{0.9}V_3O_{7.9}F_{0.1}\cdot 0.9H_2O$, which delivered an initial discharge capacity of 409 mAh g^{-1} at C/80 rate during 1.5–4.0 V versus Li but with very poor cycling life. Our research results demonstrate that $NH_4V_3O_8$ could be used as a novel and potential cathode material for Li-ion batteries. It is believed that nanostructured $NH_4V_3O_8$ could provide improved electrochemical performance, especially

* Corresponding authors. Tel.: +86 731 88879850; fax: +86 731 88879850.
E-mail addresses: wanghy419@126.com (H. Wang), klhuang@mail.csu.edu.cn (K. Huang).

0378-7753/$ – see front matter © 2011 Elsevier B.V. All rights reserved.
doi:10.1016/j.jpowsour.2011.10.069

the rate capability. Surfactants have been widely used as soft template to prepare a variety of nanostructured cathode materials [25–28].

Herein, we present one-dimensional $NH_4V_3O_8{\cdot}0.37H_2O$ nanorods with high electrochemical performance by sodium dodecyl benzene sulfonate (SDBS) assisted hydrothermal method for Li-ion batteries. The nanorods exhibit a high discharge capacity of about 332 mAh g^{-1} at 15 mA g^{-1}, associated with good cycling stability and rate capability. More importantly, in comparison with $NH_4V_3O_8$ flakes without SDBS, the nanorods here show much higher Li ions intercalation plateaus, leading to a higher discharge capacity of about 200 mAh g^{-1} with the low cut-off voltage of 2 V, which makes it more promising when used as cathode material for Li-ion battery.

2. Experimental

2.1. Synthesis

All the starting materials were analytically pure grade and used directly without any purification. In this paper, sodium dodecyl benzene sulfonate (SDBS) was used as a soft template. At first, 0.909 g NH_4VO_3 and 0.300 g SDBS were dissolved in deionized water successively and the mixture was stirred violently at about 100 °C. Then a proper amount of hydrochloric acid with the concentration of 1.2 mol L^{-1} was added into the solution to adjust the pH value to about 4.0. The mixed solution with some insoluble intermediate was then transferred into a 50 ml Teflon lined stainless steel autoclave. The total volume of the solution was about 40 ml. The autoclave was sealed and heated at 180 °C for 48 h and then cooled to room temperature naturally. The obtained precipitate was collected by centrifugation, washed with deionized water and ethanol for several times to remove the residual SDBS. Finally, $NH_4V_3O_8{\cdot}xH_2O$ nanorods were obtained after drying at 80 °C overnight.

For comparison, orange-yellow $NH_4V_3O_8{\cdot}xH_2O$ flakes were prepared by the similar hydrothermal method without adding SDBS.

2.2. Characterization

X-ray diffraction (XRD) data were collected by a Philips X-Pert system (Cu-Kα radiation) with a step of 0.02°. Fourier transform infrared (FT-IR) spectra were recorded using the Nicolet 6700 FT-IR spectrometer. Thermal gravimetry (TG) was carried out with a NETZSCH STA 449C differential scanning calorimeter under N_2 atmosphere at a ramping rate of 10 °C min^{-1}. Morphological studies were conducted using a JSM6430F scanning electron microscopy (SEM) and a JEOL JEM-2011 transmission electron microscopy (TEM) employing a LaB6 filament as the electron source and an accelerating voltage of 200 keV. N_2 adsorption–desorption analysis was carried out using a Micromeritics ASAP 2020. The typical sample weight used was about 100 mg. The outgas condition was set to 180 min at 120 °C under vacuum, and all adsorption–desorption measurements were carried out at liquid nitrogen temperature.

2.3. Electrochemical measurements

The electrochemical cells were constructed by mixing the active material, polyvinylidene fluoride (PVDF), and Super S carbon in the weight ratio of 80:10:10. Tetrahydrofuran was used as solvent. The slurry was cast onto Al foil using a Doctor-Blade technique. After solvent evaporation at room temperature and heating at 80 °C under vacuum for 8 h, the electrodes were cut into disks and assembled into CR2016 coin-type cells with commercial electrolyte (Merck; 1 M $LiPF_6$ in 1:1 v/v ethylene carbonate/dimethyl carbonate) and a Li metal as counter electrode. The cells were constructed in an Ar-filled MBraun glovebox and then cycled galvanostatically between 1.5 and 4.0 V (voltage unit in this paper is versus Li/Li^+) at a desired current density with a Land CT2001A tester system at room temperature. Cyclic voltammetry (CV) test was carried out using the electrochemical station (Shanghai Chenhua, China) with a scan rate of 0.1 mV s^{-1} at room temperature.

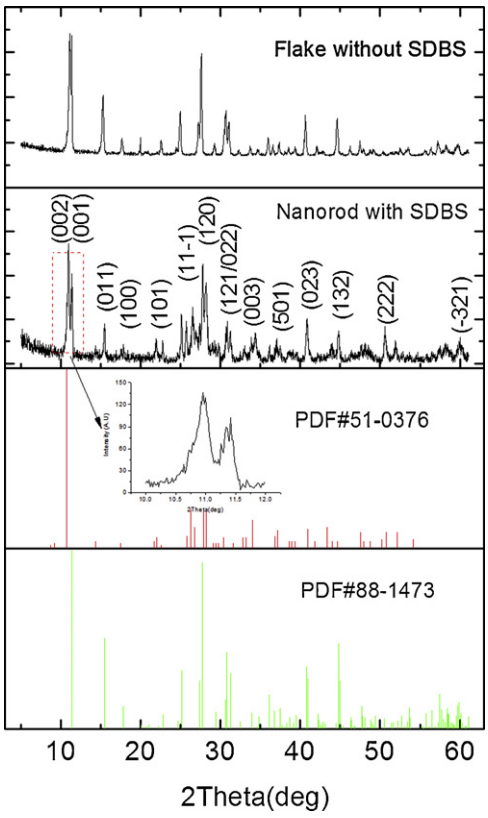

Fig. 1. XRD patterns of as-prepared materials: (a) flake without SDBS; (b) nanorod with SDBS, the standard PDF cards (no. 51-0378 and 88-1473) are attached.

3. Results and discussion

Fig. 1 illustrates the XRD patterns of as-prepared powder by hydrothermal method with SDBS and without SDBS, together with the enlarged view of that with SDBS between 10° and 12° inset. For better comparison, the standard PDF cards of no. 51-0376 ($(NH_4)_2V_6O_{16}{\cdot}1.5H_2O$) and 88-1473 ($NH_4V_3O_8$) are also attached. As seen, all the diffraction lines in XRD pattern a could be readily indexed to a monoclinic crystalline $NH_4V_3O_8$ phase (space group $P2_1/m$) with the lattice parameters $a = 0.5051$ nm, $b = 0.8439$ nm, $c = 0.8010$ nm and $\beta = 97.06°$, which are consistent well with our previous paper [21]. No peaks from other phases have been detected, indicating that the products are of high purity. It also shows the much decreased relative intensity of diffraction line (0 0 1), implying the inferior crystallinity in comparison with the standard card of 88-1473, which probably holds a promise for better Li^+ insertion/extraction ability since the preferential ordering of crystal would lead to a long Li^+ diffusion path [29]. An analogous effect is known for V_6O_{13}, where the material with short diffusion paths has a much higher capacity than the highly crystalline material with long, one-dimensional diffusion paths [30]. The sample with SDBS demonstrates much more complicated diffraction patterns. Apparently, as recorded in Fig. 1, it matches well with the diffraction patterns of two ammonium vanadate phases ($(NH_4)_2V_6O_{16}{\cdot}1.5H_2O$ and $NH_4V_3O_8$) based on the JCPDS cards (no. 51-0376 and 88-1473), revealing that the as-prepared

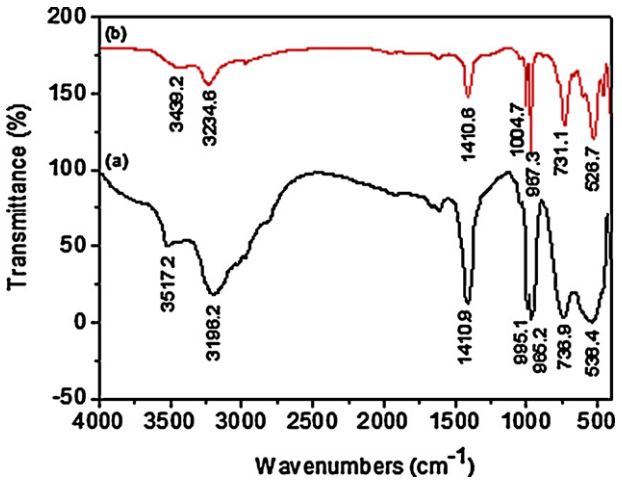

Fig. 2. FT-IR spectra of as-prepared materials: (a) nanorod with SDBS; (b) flake without SDBS.

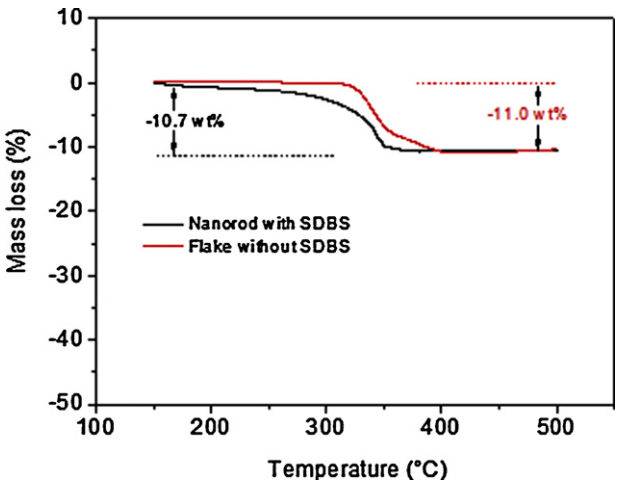

Fig. 3. TG curves of as-prepared materials: (a) nanorod with SDBS; (b) flake without SDBS.

material with SDBS is probably the composite phases of both ammonium vanadates. It is a little hard to explain why the product here shows two quite similar structure phases. But our related research suggests that $NH_4V_3O_8$ is sensitive to the experiment conditions, including pH value, reaction temperature, reaction time as well as surfactants, which play a crucial role in forming of structure and morphology for final products. It is obvious that the different phases of the flakes and the nanorods are attributed to the absence or presence of the SDBS. Nevertheless, both phases are almost the same except for the difference of crystal water. So, the complicated product could be described as $NH_4V_3O_8{\cdot}xH_2O$, which should still belong to the monoclinic system with the $P2_1/m$ space group.

FT-IR spectra provide further insight into the slight difference of internal structure of the obtained materials with and without SDBS (Fig. 2). The sample without SDBS has characteristic IR peaks at 1004.7, 967.3, 731.1 and 526.7 cm^{-1} which can be attributed to V=O stretching of distorted octahedral and distorted squarepyramids, asymmetric and symmetric stretching vibration of V–O–V bonds, respectively [31,32]. In addition, NH_4^+ group and crystal water are identified by their characteristic bands at 3235.9 and 1410.5 cm^{-1}, 3464.8 and 1612.5 cm^{-1}, respectively [33,34]. So the sample without SDBS is actually composed of $NH_4V_3O_8{\cdot}xH_2O$. The sample with SDBS shows the similar absorption IR bands, but the position and the intensity of those bands are a little different, which imply the alteration of chemical structure of the product due to the addition of surfactant SDBS. The IR spectra change further confirms the XRD results in Fig. 1. The difference has been reported [21,35].

To determine the amount of crystal water in each molecular formula, TG test of as-prepared materials without and with SDBS were carried out (Fig. 3). The difference in the weight loss and the corresponding decomposition temperature is discovered, implying the effect of SDBS on the structure of the final product. The similar phenomenon was reported in our previous work due to the addition of CNTs [21]. The mass loss is attributed to the decomposition of ammonium trivanadate, shown as the following Eq. (1):

$$2NH_4V_3O_8 \cdot xH_2O \xrightarrow{\Delta} 3V_2O_5 + 2NH_3 \uparrow + (1+2x)H_2O \quad (1)$$

Based on the mass loss of 10.7 wt% for the nanorods and 11.0 wt% for the flakes, it demonstrates that the nanorods consist of $NH_4V_3O_8{\cdot}0.37H_2O$ (it also could be written as $(NH_4)_2V_6O_{16}{\cdot}0.74H_2O$), while the flakes are composed of $NH_4V_3O_8{\cdot}0.42H_2O$. The amount of crystal water for the nanorods (0.37 per formula unit) is reasonable, which is in good agreement with the composite phases in Fig. 1. It should be pointed out that the amount of crystal water for the flakes without SDBS is a little larger than that of the nanorods. However, its structure phase is closed to the pure $NH_4V_3O_8$, rather than the $(NH_4)_2V_6O_{16}{\cdot}1.5H_2O$. In our opinion, it should be due to the absence of SDBS.

Fig. 4 shows the morphology of as-prepared materials with and without SDBS. As can be seen, the sample prepared without SDBS shows good flake-like morphology. The flakes have the width of 4–10 micrometers and the thickness of 600–900 nm, which are a little larger than that in our recent work [21]. At the same time, smooth and clean surface is observed. As for the material with the SDBS, it consists of a large quantity of uniform 1D nanorods. The diameter of the nanorods is about 30 nm and the length is less than 1 μm, some of which are only about 100 nm. The comparison result indicates that SDBS plays a key role in forming the nanorod morphology. It is believed that SDBS could act as a soft template to direct the growth of nanoparticles into nanorods at the early stage of the process through a preferential bonding to certain crystal planes. Similar work using SDBS as soft template to obtain nanostructured $LiFePO_4$ has been reported by Teng et al. [36]. Brunauer–Emmett–Teller (BET) was conducted to obtain the information of surface area. BET specific surface area of the nanorods is estimated to be 15.1 $m^2\,g^{-1}$, which is a reasonable value achievable for electrode materials and it is much larger than that (4.2 $m^2\,g^{-1}$) of the flakes. The relatively larger surface area of $NH_4V_3O_8{\cdot}0.37H_2O$ nanorod prepared using SDBS as soft template ensures particle–particle tight contact and short diffusion distances of Li ions and therefore holds the promise for enhanced Li storage performance. Note that less sodium dodecyl sulfonate (SDS) was once used in our previous work for the synthesis of $NH_4V_3O_8{\cdot}0.2H_2O$ [19]. However, the product still shows the flake morphology, almost the same with that without surfactant. It is probably due to the addition of a slight amount of SDS. As a matter of fact, the concentration of the surfactants plays an important role in controlling the morphology of the nanostructured materials [25,28].

High-resolution TEM image (HRTEM) of individual nanorod is depicted in Fig. 5. As shown in Fig. 5(a) and (c), the fringe spacings of the crystalline nanorods are 0.345 nm and 0.283 nm, which are in good accordance with plane distance of the (1 1 −1) and (0 0 3) planes, respectively, of the monoclinic layered $NH_4V_3O_8{\cdot}xH_2O$ shown in Fig. 1. HRTEM result demonstrates single crystalline nature of the nanorods and the crystal growth along the (1 1 −1) direction. However, it should be noted that the as-prepared material is beam-sensitive under an electron beam with an accelerated voltage of 200 kV. Thus, it is hard to obtain high quality HRTEM images.

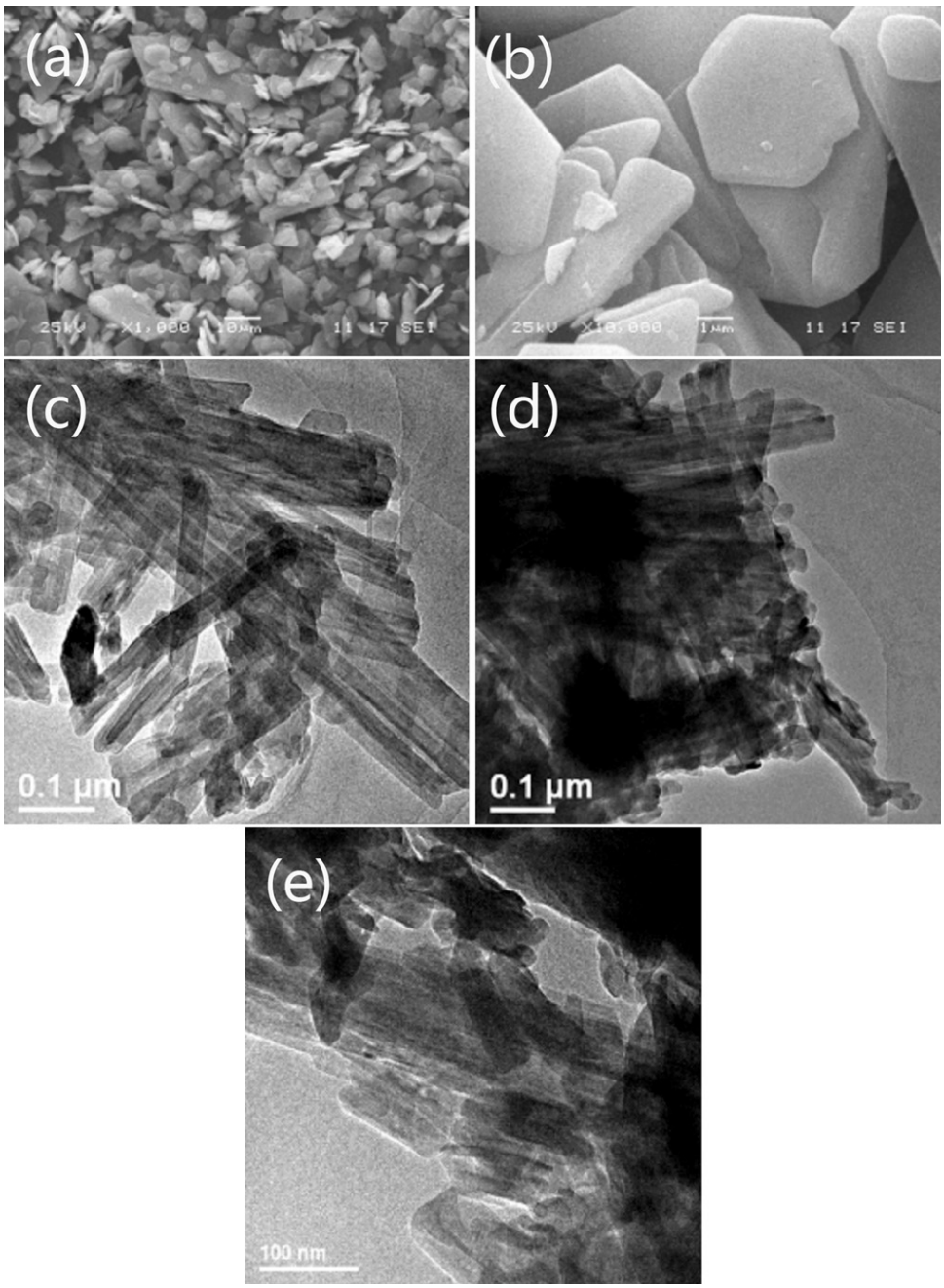

Fig. 4. SEM images of as-prepared material without SDBS (a and b) and TEM images of as-prepared material with SDBS (c–e).

Fig. 6 shows the CV curves of $NH_4V_3O_8{\cdot}0.37H_2O$ nanorods and $NH_4V_3O_8{\cdot}0.42H_2O$ flakes. It is very interesting to note that the two materials indicate significant difference in terms of the lithium ion intercalation/deintercalation behavior. Two main pairs of redox peaks with the oxidation peak at 1.84, 3.01 V and corresponding reduction peak at 1.71, 2.89 V respectively, associated with a slight one at 2.61 and 2.43 V, are observed for the sample without SDBS. It is interesting that the reduction peak at 3.01 V is much smaller than the corresponding oxidation peak, while that at 1.84 V is greatly larger, which is different from that of $NH_4V_3O_8{\cdot}0.2H_2O$ [19]. A slight structure difference should be involved for the uncommon electrochemical behavior. It further suggests that the structure of the vanadate is sensitive to the experimental conditions [37]. Vanadium oxide nanotubes (VO_x-NTs) also indicated the similar phenomenon [38]. Note that the main reduction peak, almost corresponding to the discharge plateau in the following Fig. 7, is less than 2.0 V, which means the lower energy density for this kind of material used as cathode. On the contrary, $NH_4V_3O_8{\cdot}0.37H_2O$ prepared by the SDBS assisted method shows much higher lithium ion insertion potentials. Three main pairs of redox peaks are concentrated between 2.1 and 3.0 V, with the oxidation peak at 2.58, 2.79, 3.01 V and the corresponding reduction peak at 2.34, 2.64, 2.89 V, respectively, which are similar to those of LiV_3O_8 in the literature [39]. The splitting of many redox peaks was because of the different lithium sites with energy difference for holding the lithium ions [40]. XRD, FT-IR, TG and CV results leave no doubt that the addition of SDBS affects the structure and electrochemical performance of the as-prepared product. Apparently, the nanorods with SDBS possess much better practical application and perspective as cathode material for Li-ion battery.

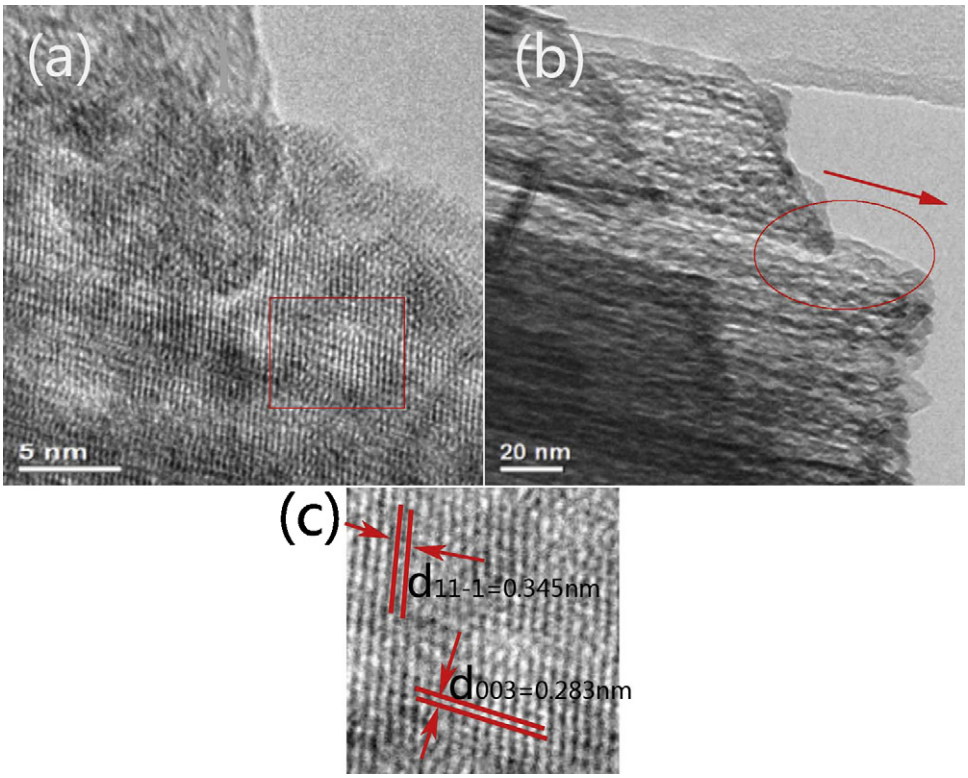

Fig. 5. High-resolution TEM image (a) and the corresponding TEM image (b) of $NH_4V_3O_8{\cdot}0.37H_2O$ nanorods, image c is the enlarged view of selective area in image (a).

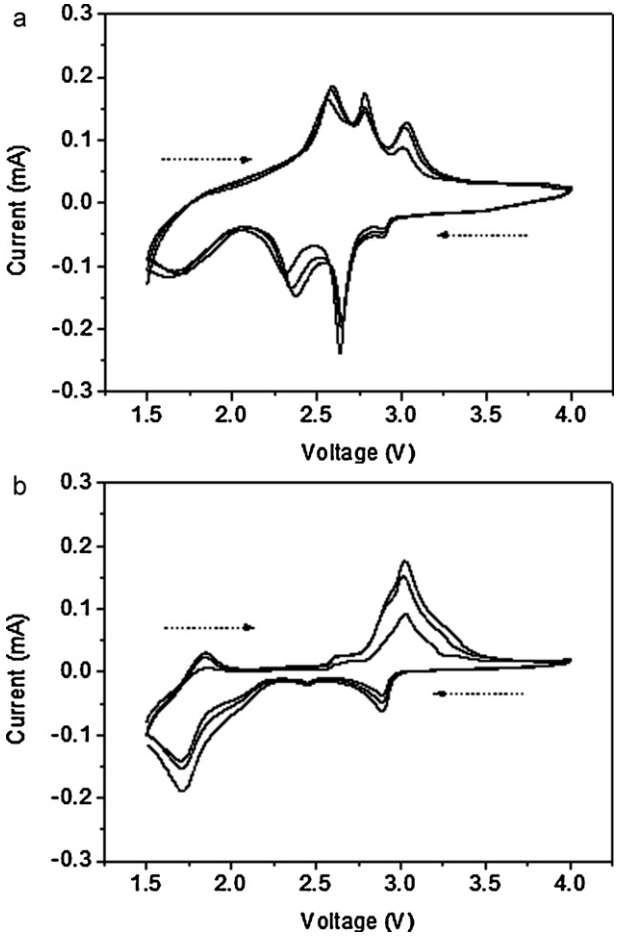

Fig. 6. Cyclic voltammetry curves of as-prepared materials: (a) nanorod with SDBS; (b) flake without SDBS, operated between 1.5 and 4.0 V at a scanning rate of 0.1 mV s^{-1}.

Fig. 7 illustrates the electrochemical performance of $NH_4V_3O_8{\cdot}0.37H_2O$ nanorods and $NH_4V_3O_8{\cdot}0.42H_2O$ flakes, associated with the first 10 discharge galvanostatic curves inset. As can be seen, the nanorods deliver a high initial discharge capacity of 308.5 mAh g^{-1} at 30 mA g^{-1}. It is increased to 327.1 mAh g^{-1} at the second cycle, which corresponds with about 3.5 lithium ions insertion into per formula unit, forming the $(NH_4)Li_{3.5}V_3O_8{\cdot}0.37H_2O$. The discharge capacity of the nanorods here is comparable to those LiV_3O_8 with high capacity [15,38,41]. A slight capacity loss is found during the following several cycles. However, it then keeps more stable with the discharge capacity of 311.7 mAh g^{-1} maintaining at the 10th cycle. As for the flakes without SDBS, it shows a much lower initial discharge capacity (206.5 mAh g^{-1}) and reaches a maximum discharge capacity of 301.3 mAh g^{-1} gradually. The phenomenon of noticeable increasing discharge capacity, also shown in our former paper, might be ascribed to the severe polarization of the electrode related to the structure [19], which could be partially explained by the discharge curves inset. We ascribe such phenomenon to a possible activation process. Undoubtedly, the nanorods suffer from the less electrochemical polarization in comparison with the bulk flakes. Both samples show very low initial charge capacity, suggesting the NH_4^+ group could not be extracted at the first charge process. It is worthwhile to highlight that the nanorods exhibit about 200 mAh g^{-1} discharge capacity to 2.0 V, while that of the flakes is less than 100 mAh g^{-1}, which agrees well with the CV results (higher discharge plateaus).

Cycling performance of the nanorods and flakes at a relatively high current density of 150 mA g^{-1} are also investigated (Fig. 8). The initial discharge capacity of the nanorods is 208.9 mAh g^{-1}, which is about 14 mAh g^{-1} higher than that of flakes. More interestingly, the nanorods exhibit much better cycling performance. The capacity increases gradually until reaching the maximum value of about 231 mAh g^{-1}, then it maintains well after 60 cycles, indicating the excellent cycling stability. On the other hand, the flakes present a discharge capacity of 181.3 mAh g^{-1} (about 93% of the initial

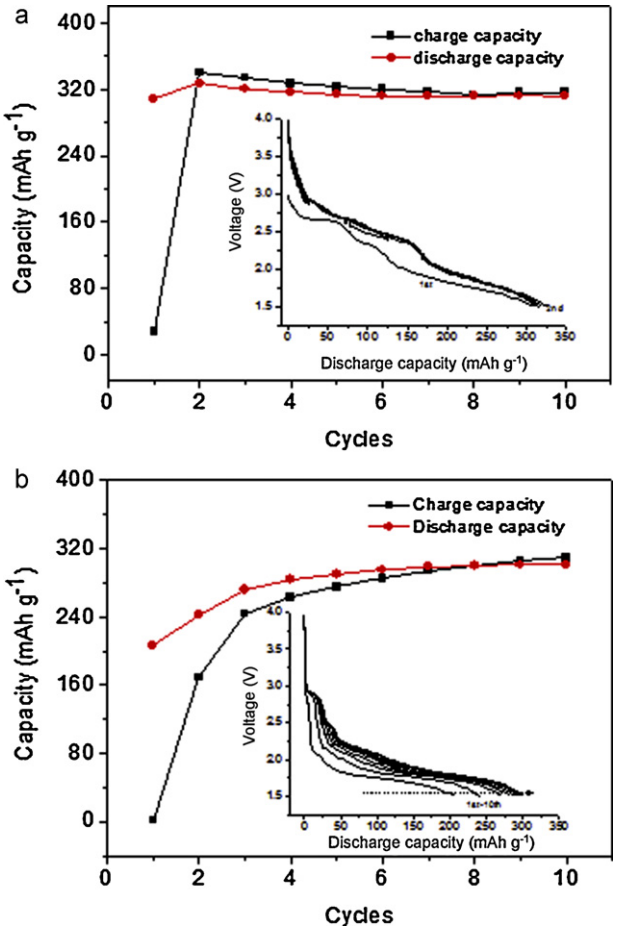

Fig. 7. Cycling performance of as-prepared materials: (a) nanorod with SDBS; (b) flake without SDBS, operated at 30 mA g^{-1} between 1.5 and 4.0 V. Inset is their discharge galvanostatic curves.

value) after 60 cycles. Both samples show much better cycling stability than $(NH_4)_{0.9}V_3O_{7.9}F_{0.1}\cdot 0.9H_2O$ [24]. Generally, the structure of LiV_3O_8 and $NH_4V_3O_8$ can be described as $V_3O_8^-$ puckered layers held together by Li^+ and NH_4^+ groups [19], respectively, which almost occupy the octahedral sites in each crystallite and acts as pillar for stabilizing the structure. Accordingly, like LiV_3O_8, $NH_4V_3O_8$ also shows good structure stability during the cycling. Anyway,

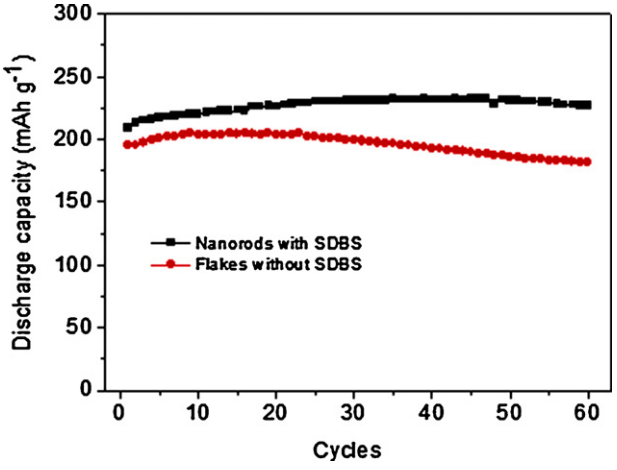

Fig. 8. Cycling performance of as-prepared materials: (a) nanorod with SDBS; (b) flake without SDBS, operated at 150 mA g^{-1} between 1.5 and 4.0 V.

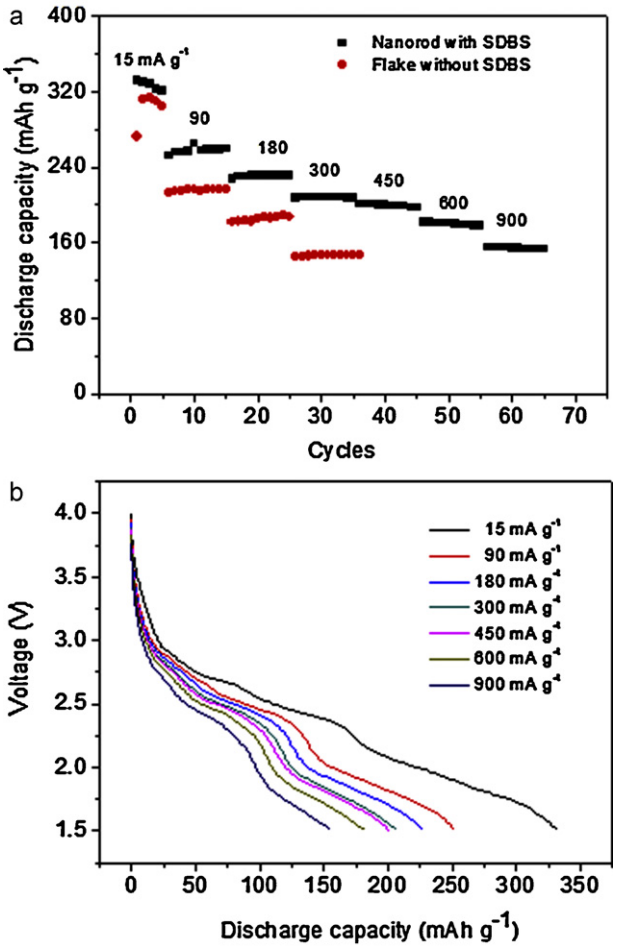

Fig. 9. Variation of discharge capacity versus cycle numbers for $NH_4V_3O_8\cdot 0.37H_2O$ nanorods and $NH_4V_3O_8\cdot 0.42H_2O$ flakes (a) and the corresponding discharge curves for the nanorods (b) at various current densities (15 mA g^{-1}, 90 mA g^{-1}, 180 mA g^{-1}, 300 mA g^{-1}, 450 mA g^{-1}, 600 mA g^{-1}, 900 mA g^{-1}) between 1.5 and 4.0 V.

results above reveal that the addition of SDBS in this work is of great importance to the melioration of lithium ion insertion/deinsertion plateaus, as well as the cycling stability for $NH_4V_3O_8$. The improved electrochemical performance should be mainly ascribed to the nanorod characteristic with much larger BET area (more than three times) and shorter Li ion diffusion path [8–10].

As an interesting cathode material candidate for lithium ion battery, the rate capability should also be considered. Fig. 9 depicts the cycling performance and the typical discharge curves of the $NH_4V_3O_8\cdot 0.37H_2O$ nanorods at various current densities from 15 to 900 mA g^{-1}. For comparison, electrochemical performance of $NH_4V_3O_8\cdot 0.42H_2O$ flakes is also given. Clearly, the specific discharge capacities of 332.3, 258.3, 230.4, 207.6, 201.2 and 181.8 mAh g^{-1} are observed for the nanorods at 15, 90, 180, 300, 450 and 600 mA g^{-1}, respectively. Even at 900 mA g^{-1}, it still maintains 155.4 mAh g^{-1} discharge capacity. While those for the flakes are 311.3, 214.8, 185.3, 146.5 mAh g^{-1} at 15, 90, 180 and 300 mA g^{-1}, respectively. Apparently, the nanorods with SDBS show much better rate capability than flakes without SDBS due to the larger BET surface area and shorter Li^+ diffusion distance [8–10]. The typical discharge curves (Fig. 9(b)) at various rates demonstrate the good lithium ion intercalation/deintercalation plateaus. It is worthwhile to note that no obvious capacity fading could be observed at relatively high rates even at 900 mA g^{-1}. Two things should be noted. One is the obvious capacity loss at 15 mA g^{-1}, which is consistent with those of LiV_3O_8 [15,39] and $NH_4V_3O_8$

[21]. It is believed that more available sites for Li ions could be used at low current density, some of which probably possess the inferior reversibility of Li^+ insertion and extraction. For example, Li^+ inserted into the octahedral sites in the interlayer is hard to be extracted. The other is the large decreasing discharge capacity when the current density increases from 15 to 90 mA g^{-1}, implying the intrinsic poor lithium ion transport ability in the vanadate system. It might be due to the existence of a large amount of crystal water. Bonino et al. [42] considered that the low diffusion coefficient of Li^+ in $Li_xV_3O_8$ was probably correlated with the residual water in the material, which could limit the lithium ion mobility by forming electrostatic bonds. However, the hypothesis is beyond the scope of this paper. We will investigate the influence of the crystal water on the electrochemical performance in our following work. Nevertheless, $NH_4V_3O_8{\cdot}0.37H_2O$ nanorods here present good rate capability and cycling stability at relatively high current density, which are comparable to the results of the best LiV_3O_8 to date [15,39]. LiV_3O_8 nanorods with a maxmium discharge capacity of 348 mAh g^{-1} at 20 mA g^{-1} was prepared by Liu et al. [15], but it decreased to *ca.* 200 mAh g^{-1} at 100 mA g^{-1}. Pan et al. [39] fabricated LiV_3O_8 nanosheet, showing the best cycling stability so far. However, the insufficient rate capability was demonstrated by the large capacity drop from 260 to *ca.* 190 mAh g^{-1} when the current density was increased from 100 to 300 mA g^{-1}.

4. Conclusions

In summary, $NH_4V_3O_8{\cdot}0.37H_2O$ nanorods with a diameter of about 30 nm were synthesized by a facile hydrothermal method using SDBS as the soft template. Crystal structure of the nanorods was a little different from the material made without SDBS. It should be noted that the addition of surfactant meliorates the lithium ion insertion/extraction plateaus. More importantly, the electrochemical performance was greatly improved owning to the nanorod morphology and probable change of structure. The nanorods showed a maximum specific discharge capacity of 327.1 mAh g^{-1} at 30 mA g^{-1}, together with good rate capability up to 900 mA g^{-1}. Good cycling performance at 150 mA g^{-1} was associated with 100% capacity retention after 60 cycles. Apparently, with the excellent lithium ion insertion/deinsertion ability, $NH_4V_3O_8{\cdot}0.37H_2O$ nanorods here could be used as a very promising cathode material for Li-ion battery.

Acknowledgements

The authors greatly appreciate the financial support from the Major State Basic Research Development Program of China (973 Program) (no. 2010CB227204), Research Foundation of Hunan Province for Ph.D Student (no. CX2010B114), Graduate Degree Thesis Innovation Foundation of Central South University. H. Wang thanks to financial support from the Chinese government scholarship.

References

[1] J.M. Tarascon, M. Armand, Nature 414 (2001) 359–367.
[2] S. Megahed, B. Scrosati, J. Power Sources 51 (1994) 79–104.
[3] M. Winter, J.O. Besenhard, M.E. Spahr, P. Novák, Adv. Mater. 10 (1998) 725–763.
[4] S.Y. Chung, J.T. Bloking, Y.M. Chiang, Nat. Mater. 1 (2002) 123–128.
[5] A.D. Tang, H.Y. Wang, K.L. Huang, B. Tan, X.L. Wang, Prog. Chem. 19 (2007) 1313–1321.
[6] J.R. Owen, Chem. Soc. Rev. 26 (1997) 259–267.
[7] H. Li, Z.X. Wang, L.Q. Chen, X.J. Huang, Adv. Mater. 21 (2009) 4593–4607.
[8] P.G. Bruce, B. Scrosati, J.M. Tarascon, Angew. Chem. Int. Ed. 47 (2008) 2930–2946.
[9] M.S. Whittingham, Chem. Rev. 104 (2004) 4271–4301.
[10] E. Hosono, T. Kudo, I. Honma, H. Matsuda, H.S. Zhou, Nano Lett. 9 (3) (2009) 1045–1051.
[11] N.A. Chernova, M. Roppolo, A.C. Dillon, M.S. Whittingham, J. Mater. Chem. 19 (2009) 2526–2552.
[12] J. Jiang, Z.X. Wang, L.Q. Chen, J. Phys. Chem. C 111 (2007) 10707–10711.
[13] H.M. Liu, Y.G. Wang, L. Li, K.X. Wang, E. Hosono, H.S. Zhou, J. Mater. Chem. 19 (2009) 7885–7891.
[14] C.K. Chan, H.L. Peng, R.D. Twesten, K. Jarausch, X.F. Zhang, Y. Cui, Nano Lett. 7 (2007) 490–495.
[15] H.M. Liu, Y.G. Wang, K.X. Wang, Y.R. Wang, H.S. Zhou, J. Power Sources 192 (2009) 668–673.
[16] G.Q. Liu, C.L. Zeng, K. Yang, Electrochim. Acta 47 (2002) 3239–3243.
[17] S. Panero, M. Pasquali, G. Pistoia, J. Electrochem. Soc. 130 (1983) 1225–1227.
[18] H.Y. Xu, H. Wang, Z.Q. Song, Y.W. Wang, H. Yan, M. Yoshimura, Electrochim. Acta 49 (2004) 349–353.
[19] H.Y. Wang, K.L. Huang, S.Q. Liu, C.H. Huang, W.J. Wang, Y. Ren, J. Power Sources 196 (2011) 788–792.
[20] H.Y. Wang, K.L. Huang, C.H. Huang, S.Q. Liu, Y. Ren, X.B. Huang, J. Power Sources 196 (2011) 5645–5650.
[21] H.Y. Wang, K.L. Huang, Y. Ren, X.B. Huang, S.Q. Liu, W.J. Wang, J. Power Sources 196 (2011) 9786–9791.
[22] S.D. Huang, Y.K. Shan, Chem. Commun. 106 (1998) 9–1070.
[23] B.Z. Lin, S.X. Liu, Acta Cryst. C55 (1999) 1961–1963.
[24] C.C. Torardi, C.R. Miao, Chem. Mater. 14 (2002) 4430–4433.
[25] F.Y. Cheng, Z.L. Tao, J. Liang, J. Chen, Chem. Mater. 20 (3) (2008) 667–681.
[26] S.L. Chou, J.Z. Wang, J.Z. Sun, D. Wexler, M. Forsyth, H.K. Liu, D.R. MacFarlane, S.X. Dou, Chem. Mater. 20 (22) (2008) 7044–7051.
[27] H.Y. Wang, K.L. Huang, S.Q. Liu, Y. Luo, Chin. J. Inorg. Chem. 25 (2009) 2090–2096.
[28] A. Hintennach, P. Novák, Phys. Chem. Chem. Phys. 11 (2009) 9484–9488.
[29] G. Pistoia, M. Pasquali, G. Wang, L. Li, J. Electrochem. Soc. 137 (1990) 2365–2370.
[30] D.W. Murphy, P.A. Christian, F.J. DiSalvo, J.N. Carides, J.V. Waszczak, J. Electrochem. Soc. 128 (1981) 2053–2060.
[31] B. Azambre, M.J. Hudson, O. Heintz, J. Mater. Chem. 13 (2003) 385–389.
[32] H.Q. Li, T.Y. Zhai, P. He, Y.G. Wang, E. Hosono, H.S. Zhou, J. Mater. Chem. 21 (2011) 1780–1787.
[33] A. Dobley, K. Ngala, S.F. Yang, P.Y. Zavalij, M.S. Whittingham, Chem. Mater. 13 (2001) 4382–4386.
[34] L.Q. Mai, C.S. Lao, B. Hu, J. Zhou, Y.Y. Qi, W. Chen, E.D. Gu, Z.L. Wang, J. Phys. Chem. B 110 (2006) 18138–18141.
[35] J. Kawakita, T. Miura, T. Kishi, Solid State Ionics 124 (1999) 29–35.
[36] F. Teng, S. Santhanagopalan, A. Asthana, X.B. Geng, S. Mho, R. Shahbazian-Yassar, D.D. Meng, J. Cryst. Growth (2010), doi:10.1016/j.jcrysgro.2010.09. 005.
[37] J. Livage, Materials 3 (2010) 4175–4195.
[38] A.I. Popa, E. Vavilova, C. Täschner, V. Kataev, B. Büchner, R. Klingeler, J. Phys. Chem. C 115 (2011) 5265–5270.
[39] A.Q. Pan, J. Liu, J.G. Zhang, G.Z. Cao, W. Xu, Z.M. Nie, X. Jie, D. Choi, B.W. Arey, C.M. Wang, S.Q. Liang, J. Mater. Chem. 21 (2011) 1153–1161.
[40] J. Kawakita, M. Majima, T. Miura, T. Kishi, J. Power Sources 66 (1997) 135–139.
[41] S.H. Ju, Y.C. Kang, Mater. Chem. Phys. 126 (2011) 133–137.
[42] F. Bonino, S. Panero, M. Pasquali, G. Pistoia, J. Power Sources 56 (1995) 193–196.